Acta Scientiarum
http://periodicos.uem.br/ojs/acta
ISSN on-line: 1807-8664
Doi: 10.4025/actascitechnol.v42i1.45703

Flow-velocity model for hydrokinetic energy availability assessment in the Amazon

Josias da Silva Cruz[1], Claudio José Cavalcante Blanco[2*] and Antônio César Pinho Brasil Junior[3]

[1]Programa de Pós-Graduação em Engenharia Civil, Universidade Federal do Pará, Rua Augusto Correa, 01, 66075-110, Belém, Pará, Brazil. [2]Faculdade de Engenharia Sanitária e Ambiental, Belém, Universidade Federal do Pará, Pará, Brazil. [3]Departmento de Engenharia Mecânica, Campus Universitário Darcy Ribeiro, Universidade de Brasília, Brasília, Distrito Federal, Brazil. *Author for correspondence. E-mail: blanco@ufpa.br

ABSTRACT. The Brazilian hydrological information network does not provide data series of daily velocities. The river velocities are important for the study of hydrokinetic potential. Therefore, the work proposes a model called flow-velocity that estimates the average daily velocity and the distribution of the velocity profile of the cross section of rivers. The model was applied to the Amazon basin, using the highest and lowest flow rates of the historical series. The highest and lowest average velocities found in the Amazon River were 2.27 m s^{-1} and 0.735 m s^{-1}, respectively. The main contributors to the Amazon River presented average daily velocities close to 2.0 ms-1 for the flood period, but in the dry season these velocities did not exceed 0.5 m s^{-1}. Thus, it was verified that the Amazon River has hydrokinetic potential throughout the year and its tributaries during the flood period.

Keywords: hydrokinetic turbines; inventory of velocity; geometric form, Amazon.

Received on December 6, 2018
Accepted on May 7, 2019

Introduction

The society searches for renewable and sustainable energy sources to meet growing demands, hydrokinetic plants have received attention in the same proportion (Petrie, Diplas, Gutierrez, & Nan, 2014). Another important factor that has led the scientific community to research alternative energy sources the search for the minimization of the environmental impacts caused by fossil fuels. Thus, the use of energy from marine and fluvial currents has been preeminent in this context (Lopes, Vaz, Mesquita, Mesquita, & Blanco, 2015). The use of hydrokinetic energy in all its applications is considered as a process of energy conversion with low environmental impact, which could increase the energy potential of countries, especially those in development that need energy to overcome the challenges of growth (Holanda et al., 2017). Within this scenario, each country is assessing its resources and many have recognized hydrokinetic energy as a significant contributor to their renewable energy portfolio (Laws & Epps, 2016).

In Brazil, according to Van Els and Brasil Junior (2015), starting in the 1980s, the first empirical research on the development of electric energy production using hydrokinetic turbines began. Currently, studies have verified the use of the remaining energy from hydroelectric plants. In this sense, Holanda et al. (2017) presented in their work a shallow water model to verify the hydrokinetic energy use downstream of the Tucuruí hydroelectric power plant in the State of Pará, Brazilian Amazonia, since it has the largest installed capacity in the national territory; and during its implantation caused a great environmental impact. According to these authors, the implantation of a hydrokinetic energy park, in the evaluated section, could generate 2.04 GWh / year, which is a considerable value for an unused energy resource.

According to Pektas (2015), the determination of velocity distributions throughout the cross section is necessary for the planning of the geometric forms of the channels; the calculation of flow properties; and the forecast of sediment transport and contaminants. However, according to Bonakdari (2012), the measurements of direct velocities are not feasible in many real cases. The National Water Agency (ANA, 2017) provides the hydrological data series (flow, water level, sediment concentration, etc.). However, the river velocity data series are not available. The reasons for this are diverse, ranging from the high financial costs to the difficulty of access to the study area.

According to Farina et al. (2017) and Maghrebi (2006), the flow of a river can be calculated by the product of the average velocity with the cross-sectional area. Therefore, depth measurement is required to

determine the cross-sectional area and determine the average velocity. According to Sivapragasam and Muttil (2005), the flows are calculated from the velocity measurement and are related to the measures of linimetric rules to obtain a key curve. Thus, a power law equation is obtained to estimate the flow rate, with the known water level being the known variable, since according to Maghrebi and Ahmadi (2017), it is more difficult to measure river flow than the level.

There are many variables that govern the equations describing the flow of a river, other than artificial channels having well defined cross-sectional geometry, declivity and roughness. In rivers, these variables are difficult to estimate because they vary in time and space. According to Rahimpour (2017), the velocity component describes the flow of the river, but the velocity in a cross section varies from one point to another. For decades, the velocity distribution in rivers has been researched (Maghrebi & Rahimpour, 2005). Therefore, the literature includes many experimental and analytical studies conducted to determine the velocity distribution in natural and laboratorial channels (Pektas, 2015). However, in most cases, the velocity profiles in rivers are expressed by a logarithmic or power law (Lee, Lee, Kim, Kim, & kim, 2013). According to Maghrebi (2006) and Petrie et al. (2014), the velocity distribution in a two-dimensional flow over a totally rough bed usually follows the logarithmic law.

Therefore, due to the importance of knowing the velocity values in rivers for many studies of water resources and hydraulic projects, especially those of hydrokinetic energy generation, the objective of the study is to develop a methodology for the design of a flow-velocity model for estimates of average daily velocity in river cross sections from flowrate data for analyse the hydrokinetic potential. Thus, this model contributes to the determination of the velocity distribution throughout the cross section of the river and estimation of the average daily velocity.

Material and methods

The model was developed by which it is possible to calculate the average daily velocity from the flow, according to the logical sequence presented in Figure 1.

The cross-sectional area was estimated using the width (z) and depth (y), which are determined randomly. Thus, the mean velocity was calculated with the use of the Continuity Equation (Equation 1) solved for this variable.

$$\overline{U} = \frac{Q}{A_e} \quad (1)$$

where: $\overline{U}$ is the average velocity, Q is the flow, and Ae is the estimated area.

According to Maghrebi (2006), the average velocity of a channel is approximately equal to that at 60% depth from the water surface. Therefore, considering the average velocity found with Equation 1 as if it were measured at 60% depth (y), the shear velocity (u*) is calculated using the logarithmic law (Equation 2). By fixing the variables y_0 and u_* and using the logarithmic law, the velocity profiles were calculated throughout the cross section according to the number of verticals. We chose the use of the logarithmic law for the determination of the velocities distribution because it is a consolidated equation in the literature (Lee et al., 2013; Babaeyan-Koopaei, Ervine, Carling, & Cao, 2002; Chen, Wang, Liu, Wang, & Leng, 2016).

$$\frac{u}{u_*} = \frac{1}{k}\ln\left(\frac{y}{y_0}\right) \quad (2)$$

with

$$y_0 = k_s e^{kA} \quad (3)$$

where: u is the local velocity measured at the normal distance y from the bed; $u_* = \sqrt{\tau_0/\rho}$ is the shear velocity at the boundary, where τ_0 is the shear stress limit and ρ is the specific mass of the water; y_0 is the boundary distance of the wall, u = 0, and k is the Von-Kármán constant = 0.41; k_s is the equivalent sand roughness height of Nikuradse = $2d_{50}$ and d_{50} is the mean diameter of the bed material; and A is the integration constant = 8.5 for a fully developed flow.

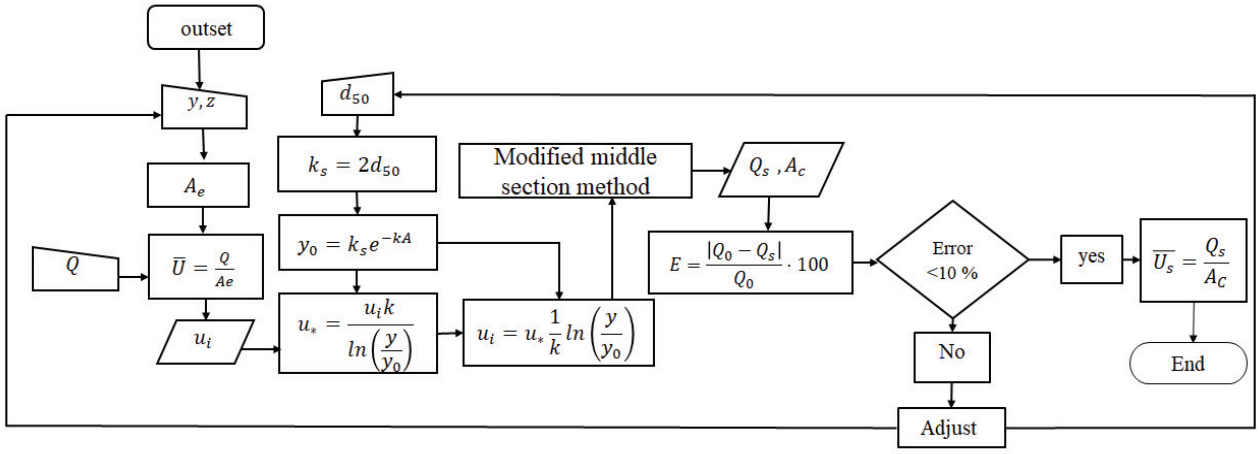

Figure 1. Flow-velocity model flowchart.

Boundary conditions

In this model, the mean velocity calculated from the continuity equation was considered a point velocity measured at the centre of the free channel at a depth of 60% from the surface. The roughness of the bed will be considered uniform. Due to the non-slip condition, the velocity along the wet perimeter is zero. The shear rate will be considered uniform throughout the cross section.

Calibration

The model calibration consists of comparing the simulated flow rate with the observed flow rate, so that the percentage relative error is less than or equal to 10%. For the flow simulation, the Modified Average Section method was used. This method uses the logarithmic velocity profiles, the depth (yi) and the subarea (ai) of the cross section (Equation 4), as shown in Figure 2. Thus, the horizontal axis of the cross section was divided into segments (zi) of a meter, regardless of the width of the cross section, because in the traditional method, the division of the segments depends on the width.

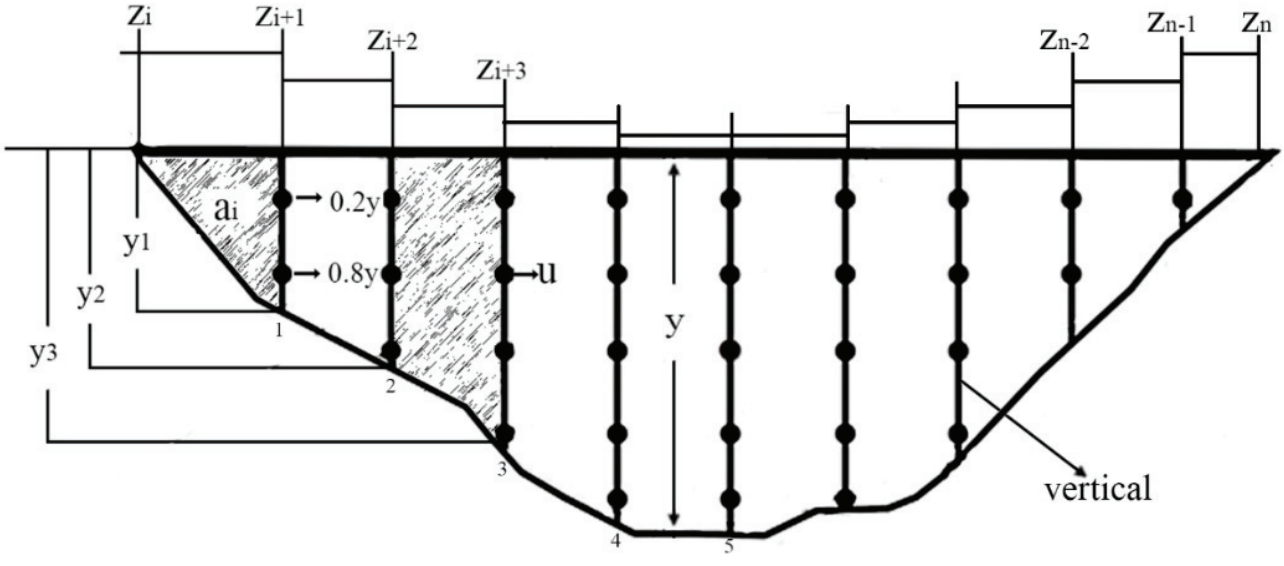

Figure 2. Illustration of the Modified Average Section method showing the subarea (a_i), the depth (y), the point velocity (u) derived from the logarithmic law and the segments (z_i).

$$a_i = \frac{\left(y_{i+1} + y_i\right)\left(z_{i+1} - z_i\right)}{2} \quad (4)$$

Thus, making use of the velocities calculated at 0.2y and 0.8y, the average between them is calculated; in this way, each vertical will have a mean velocity. Therefore, the average velocity acting on the subarea is found via Equation 5.

$$u_{ai} = \frac{u_{yi} + u_{yi+1}}{2} \quad (5)$$

where: u_{a_i} is the average velocity in the subarea, and u_{y_i} and $u_{y_{i+1}}$ are the average velocities in the vertical.

Thus, by summing the product of the average velocity in the subarea, determined the simulated flow (Q_s) was determined, according to Equation 6.

$$Q = \sum_{i}^{n} a_i u_{ai} \quad (6)$$

When the Relative Error (Equation 7) between the observed (Q_o) and simulated (Q_s) flow is less than 10%, the average velocity is calculated using Equation 8. If not, it returns to the beginning (Figure 1) and the adjustment is made in one of the variables: d_{50}, when the error is not very high; depth, the adjustment is made in this variable when the percentage error is very high; width, when the error is too high and there is no further possibility of adjustment by the depth variable.

$$E = \frac{|Q_o - Q_s|}{Q_o} \times 100 \quad (7)$$

$$\overline{U}_{\text{mod}} = \frac{Q_s}{A_c} \quad (8)$$

Area of application of the model

The flow-velocity model was applied to the Amazon River basin, and the locations of the streamflow gauge stations used in the study are shown in Figure 3. The flow data of these stations are available at http://www.snirh.gov.br/hidroweb/publico/apresentacao.jsf and were used to calibrate the model and simulate the logarithmic velocity profiles. In rivers where there are hydroelectric power plants (HPPs), preference was given to the flow data of the stations downstream of the dams, such as in the work of Holanda et al. (2017), which analysed the hydrokinetic potential of the downstream reservoir of Tucuruí HPP in the Tocantins / Araguaia basin. However, in cases where the historical series of the streamflow gauge stations located at these points were not available, upstream stream gauge stations were used. From the historical series flow rates, the highest and lowest flow values were used.

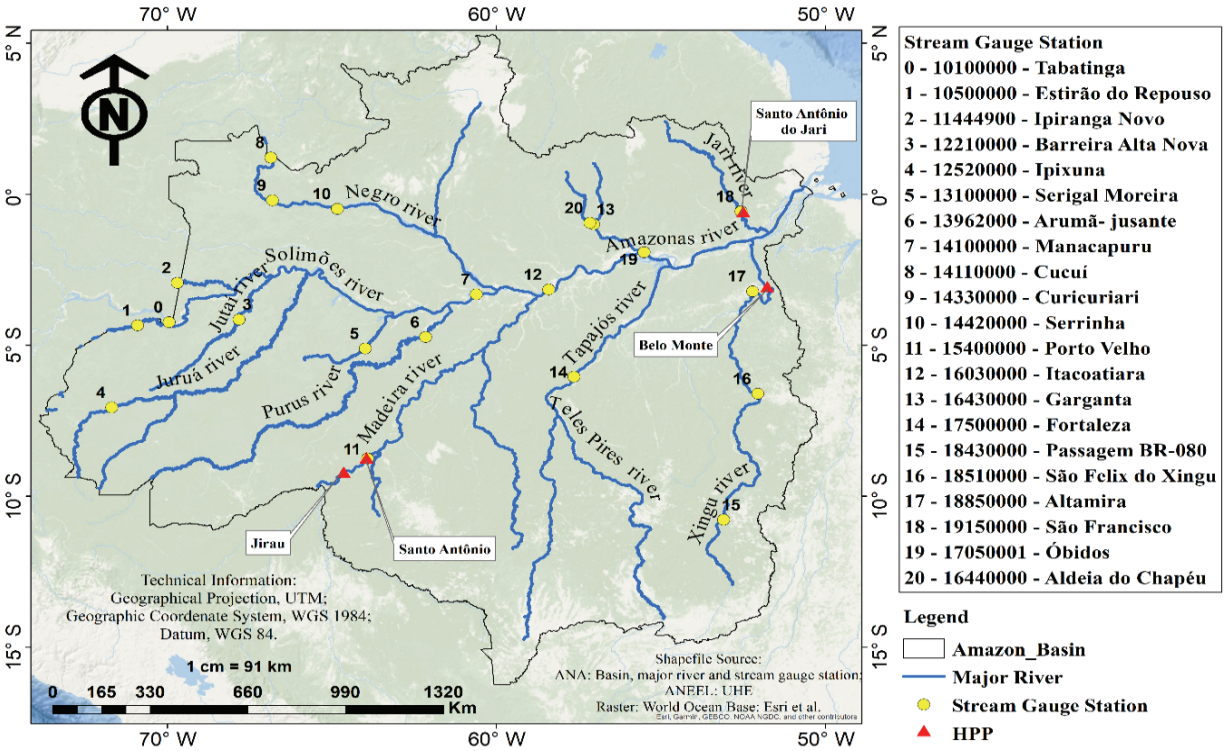

Figure 3. Locations of the streamflow gauge stations used in the flow-velocity model.

Hydrokinetic Potential Estimation

The velocity and depth of rivers is a parameter that allows the dimensioning of the rotor diameter in a hydrokinetic turbine design (Punys et al., 2015). The installed power of the plant, which varies from cube to velocity, is determined as a function of the turbine design velocity, which is a function of the velocity field of the water flow. According to Kumar and Sarkar (2016), the output power of the turbine is affected mainly by three factors: velocity, turbine rotor area, and general efficiency of the conversion system (Equation 9).

$$p = \frac{1}{2}\rho A U^3 C_p \quad (9)$$

where: P is the hydraulic power (W); ρ is the specific mass of the water (kg m^{-3}); A is the area swept by the rotor blades (m^2); U is the water velocity (m s^{-1}); and Cp is the power coefficient (Betz coefficient).

According to Kumar and Sarkar (2016) and Yuce and Muratoglu (2015), the maximum efficiency that an ideal turbine can attain is known as the Betz limit. Betz's law proposes that the theoretical maximum power coefficient for a rotating turbine in fluid flow is 0.593. However, according to Vermaak, Kusakana, and Koko (2014), the small turbines in rivers have their own losses, reducing the power coefficient to 0.25. Thus, the hydrokinetic potential was analysed for Cp = 0.593 (Betz, 1926), since according to Kumar and Sarkar (2016), this value is the maximum efficiency that an ideal turbine can reach and Cp = 0.25 is the efficiency that the small turbines in rivers can reach (Vermaak et al., 2014). In this way, two hydrokinetic potential scenarios were analysed for the studied rivers. The diameter of the rotor needed to calculate the swept area was determined as a function of the estimated depth for the lowest flow. Considering the submersion of the turbine during a drought, for the production of energy during 365 days of the year, the suggestion of Kolekar and Banerjee (2015) was considered. In this case, the end of the rotor must be within a radius of the solid surface of the river and a half radius of the free surface.

Results and discussion

Calibration

Figure 4 shows the small dispersion between the observed and simulated flows of the streamflow gauge stations shown in Figure 3. In this case, the percentage relative errors calculated through Equation 7 did not exceed 10%. With this satisfactory performance, the average velocities, for each streamflow gauge station, were simulated through Equation 8 and compared to the observed mean velocities (Figure 5). Comparative to our results, Farina et al. (2017) used an isovel model to calculate the flow of a channel with a method based on the principle of entropy and determined a relative error of 7% between observed and simulated flows, which led them to state that the velocity obtained by isovels allows a reliable flow estimation. In the study by Maghrebi, Ahmadi, Attari, and Maghrebi (2016), the maximum relative errors of 3, 6, and 3% for the Severn, Cuenca, and Tomebamba Rivers, respectively, demonstrated that the proposed model for determining the key curve presented very good performance.

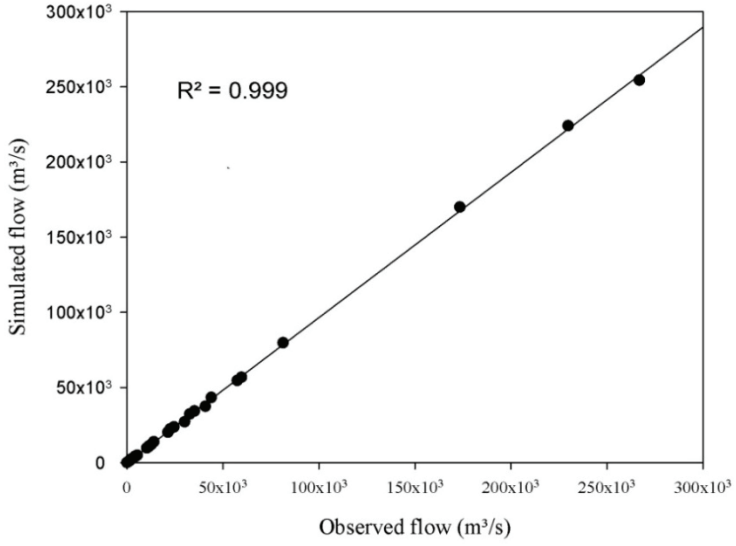

Figure 4. Correlation between the observed flow rates and those simulated by the model.

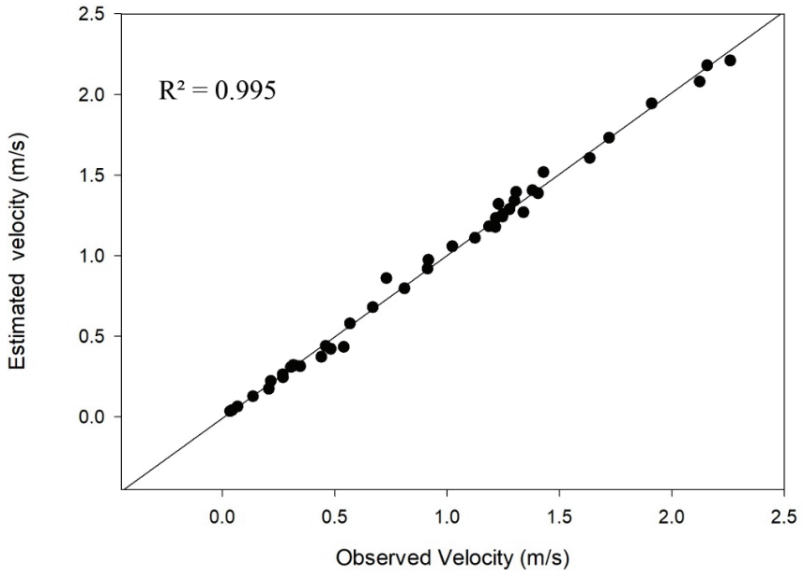

Figure 5. Correlation between the observed velocity rates and those simulated by the model.

Application of the model to the Amazon basin

The good performance of the model verified through Figures 4 and 5 allowed its use for simulations of the velocity isolines for the cross sections of the streamflow gauge stations of the Amazon River and its main tributaries of the North (Trombetas and Jari) and South (Madeira, Tapajós, and Xingu), considering the recorded historical maximum and minimum flows. These velocity distributions together with the cross-section geometry subsidize the definition of the hydrokinetic potential.

Amazon River

Figure 6 presents the velocity isolines for the cross section of the Amazon River, which were generated from a flow rate of 266,897.0 $m^3 s^{-1}$, observed at the Óbidos station (code ANA: 17050001) located in the municipality of Óbido, Pará State, Brazil. This station was taken, since it is the closest station to the mouth of the Amazon and records the highest flows of the river.

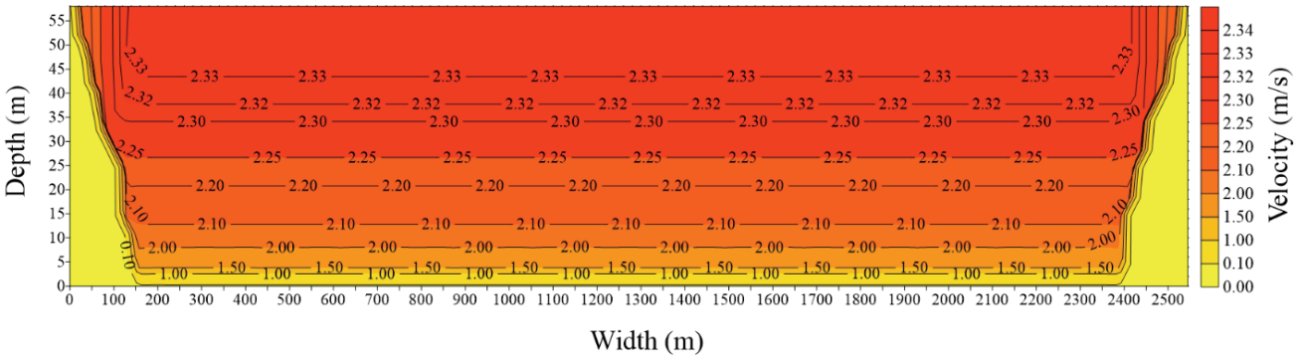

Figure 6. Velocity isolines of the cross section of the Obidos station, Amazon, at a flow of 266,897.0 $m^3 s^{-1}$.

By analysing this figure, it is possible to visualize that the lower velocities occur near the banks and the riverbed, and moving away from these regions, the velocity increases. Thus, for this type of geometric section, where the width is greater than the depth, the higher velocities are at the centre and near the surface. Farina et al. (2017), Goring, Walsh, Rutschmann, and Trösch (1997), and Maghrebi and Rahimpour (2005), using different models, found a similar velocity behaviour in rivers and artificial channels with the same geometric aspect as that studied here. The simulated Amazon River flow in Óbidos was 254,379.6 $m^3 s^{-1}$, presenting an error of 4.7% in relation to the observed flow. Influenced by this satisfactory error, the mean simulated velocity in the same section was 2.18 m s^{-1}, which is a very approximate value of the mean velocity of 2.16 m s^{-1} recorded in the data measured by ANA (National Water Agency of Brazil).

Figure 7 shows the velocity isolines of the cross section of the Amazon River (Óbidos station) at a flow rate of 59,678.0 $m^3 s^{-1}$. The velocity profile presents the same behaviour as the one with the highest flow rate. This fact is attributed to the roughness of the riverbed, which is the same for the two velocity profiles and is consistent with the literature (Keulegan, 1938; Maghrebi & Ahmadi, 2017; Pektas, 2015; Rahimpour & Maghrebi, 2006), which stated that the river and channel velocities are influenced by the bed material. The relative percentage error between the observed and simulated flow, equal to 56,971.9 $m^3 s^{-1}$, is 4.8%; thus, the resulting estimated mean velocity is 0.58 m s^{-1}. According to the ANA data, the average velocity for the flow used is 0.57 m s^{-1}, indicating a good performance of the model.

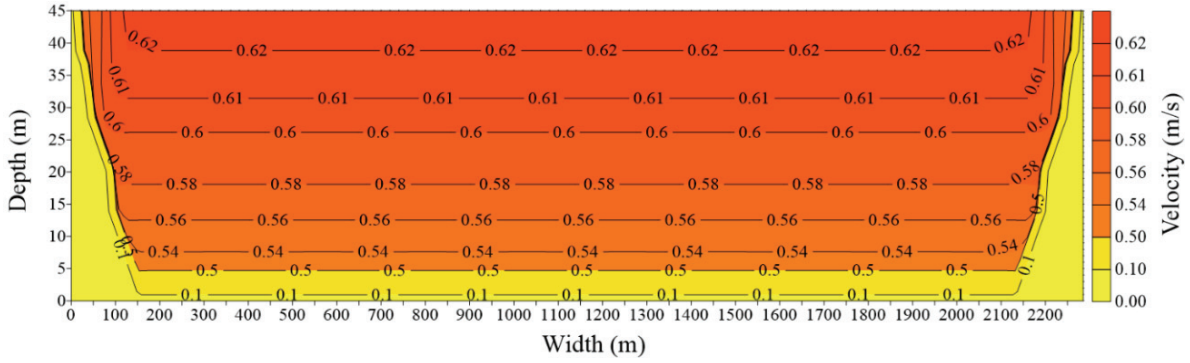

Figure 7. Isolines of the cross section of the Óbidos station, Amazon River, at a flow of 59,678.0 $m^3 s^{-1}$.

Table 1 presents the results of the application of the model to the gauge stations of Tabatinga. Itacoatiara and Manacapuru, which are also located on the Amazon River (Figure 3), but drain smaller areas when compared to the Óbidos station. Although the cross section of Tabatinga shows lower flows in relation to Itacoatiara, Manacapuru, and Óbidos, it presents higher velocities. This fact can be explained in part by the declivity, because this station is located in a terrain where the slope is greater than the other stations. In the study by Bjerklie (2007), the slope of the channel and the lengths of the meanders are used to develop an equation to estimate the velocity; the data presented in his work show that the velocity is directly proportional to the slope.

Table 1. Results of the use of the flow-velocity model in the cross sections of the streamflow gauge stations of Tabatinga, Itacoatiara, and Manacapuru.

Streamflow gauge station	Q_o ($m^3 s^{-1}$)	Q_s ($m^3 s^{-1}$)	Error (%)	U_o (m s^{-1})	U_s (m s^{-1})	Error (%)
Tabatinga	57,470.2	54,588.9	5.0	2.12	2.08	2.1
	21,362.0	20,185. 0	5.5	1.34	1.27	5.4
Itacoatiara	229,795.0	224,157.9	2.5	1.64	1.61	1.8
	81,378.0	79,703.2	2.1	0.81	0.80	1.7
Manacapuru	173,382.0	170,012.9	1.9	1.91	1.94	1.7
	43,938.3	43,331.7	1.4	0.92	0.97	6.1

Q_o – observed flow; Q_s – simulated flow, U_o – observed mean velocity and U_s – simulated mean velocity.

The simulated mean velocity values for the Itacoatiara, Manacapuru, and Óbidos stations are consistent with the values of 1.5, 1.4, and 1.7 m s^{-1}, respectively, found by Filizola, Melo, Armijos, and McGlynn (2015) for the same stations. In addition, the comparison between the simulated and observed values presents small errors.

Main tributaries of the Amazon River

North

Figure 8A and B show the profile of velocities of the Negro River, both of which are generated, respectively, from the flows of 24,509.2 $m^3 s^{-1}$ and 1,251.0 $m^3 s^{-1}$. The maximum velocities (1.5 m s^{-1} and 0.27 m s^{-1}) are close to the surface and the mean velocities (1.39 m s^{-1} and 0.22 m s^{-1}) are approximately at 60% depth from the river surface, respectively. According to the data from the Curicuriari station (code: 14330000), available at the ANA website, the mean velocities observed for these flows are, respectively, 1.31 m s^{-1} and 0.22 m s^{-1}.

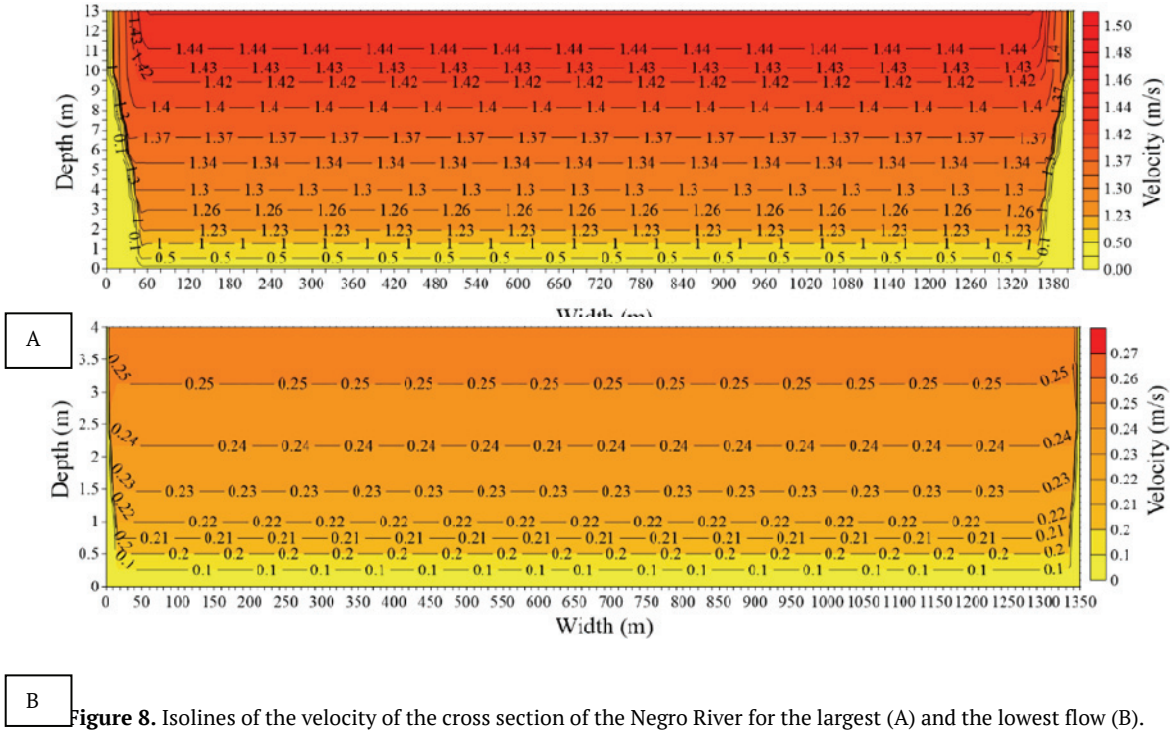

Figure 8. Isolines of the velocity of the cross section of the Negro River for the largest (A) and the lowest flow (B).

Figure 9A and B show the velocity profiles of the Trombetas River that were derived from the flow rates of 4,592.43 $m^3 s^{-1}$ and 47.0 $m^3 s^{-1}$, respectively. For the higher flow rate, the simulated mean velocity (1.29 m s^{-1}) was slightly different from that observed (1.28 m s^{-1}). For the lower flow, the simulated mean velocity (0.04 m s^{-1}) is the same as that observed.

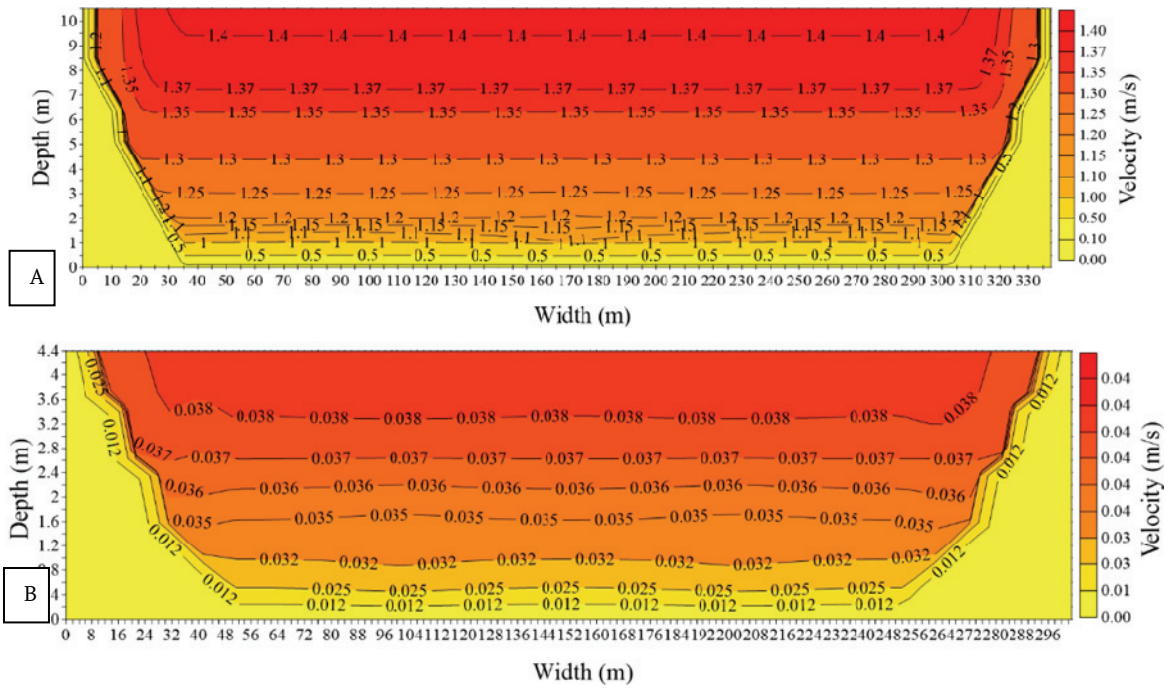

Figure 9. Velocity isolines of the cross section of the Trombetas River for the largest (A) and for the lowest flow (B).

The Trombetas River presents a high velocity for the flood period, even though it does not have such a large flow, when compared to the great tributaries of the Amazon River, which can be explained by its location in the Guiana plateau (Filizola & Guyot, 2011) and its geometric conformation (width and depth), which is the smallest among the main tributaries of the Amazon River. However, for the lower flow rate, it presents a lower velocity among the studied rivers. This peculiarity is due to the effect of backwater caused by the tide in the Amazon River, as described in the work of Kosuth et al. (2009), thus influencing its tributaries (Meade, Rayol, Conceição, & Natividade, 1991), especially those closest to the ocean. According

to Holdefer and Severo (2015), the phenomenon may be imperceptible in higher flow conditions; however, at low flow, it is noticeable.

Figure 10A and B show the velocity isolines of the Jari River, which were generated, respectively, with flows of 3,866.6 $m^3 s^{-1}$ and 52.0 $m^3 s^{-1}$. The mean velocities simulated with the above flows were 1.18 m s^{-1} and 0.04 m s^{-1}, and these values are compatible with the observed mean velocities (1.19 m s^{-1} and 0.04 m s^{-1}) for the same flows, respectively.

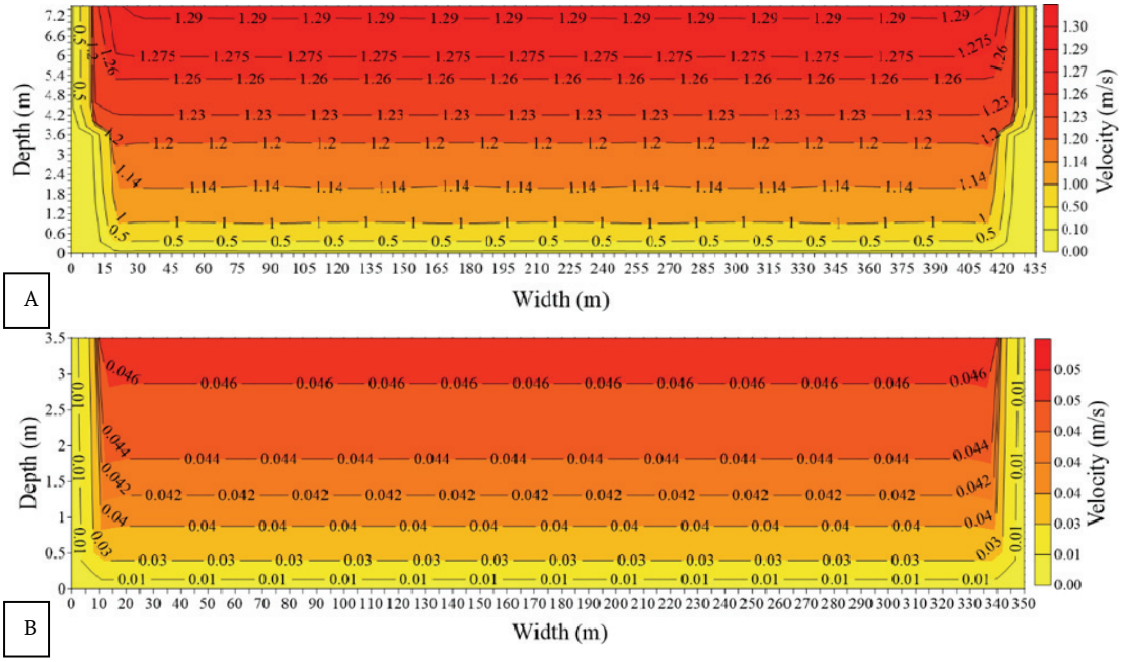

Figure 10. Isolines of the velocity of the cross section of the Jari River for the largest (A) and for the lowest flow (B).

South

Figure 11A and B show the velocity isolines of the cross section of the Madeira River. For the flow rate of 40,892 $m^3 s^{-1}$, it reaches a velocity of 2.4 m s^{-1} close to the surface and a distance of approximately 90 m from the riverbank to the middle of the river (Figure 11A). In their study, Barros and Rosman (2018) found results of superficial velocities (0.1 to 3.0 m s^{-1}), for the month of greatest peak flow, similar to this one. Simulated mean velocities are 2.21 m s^{-1} and 0.44 m s^{-1}, and the observed mean velocities recorded in the Palmeiral station are 2.26 m s^{-1} and 0.46 m s^{-1}, respectively.

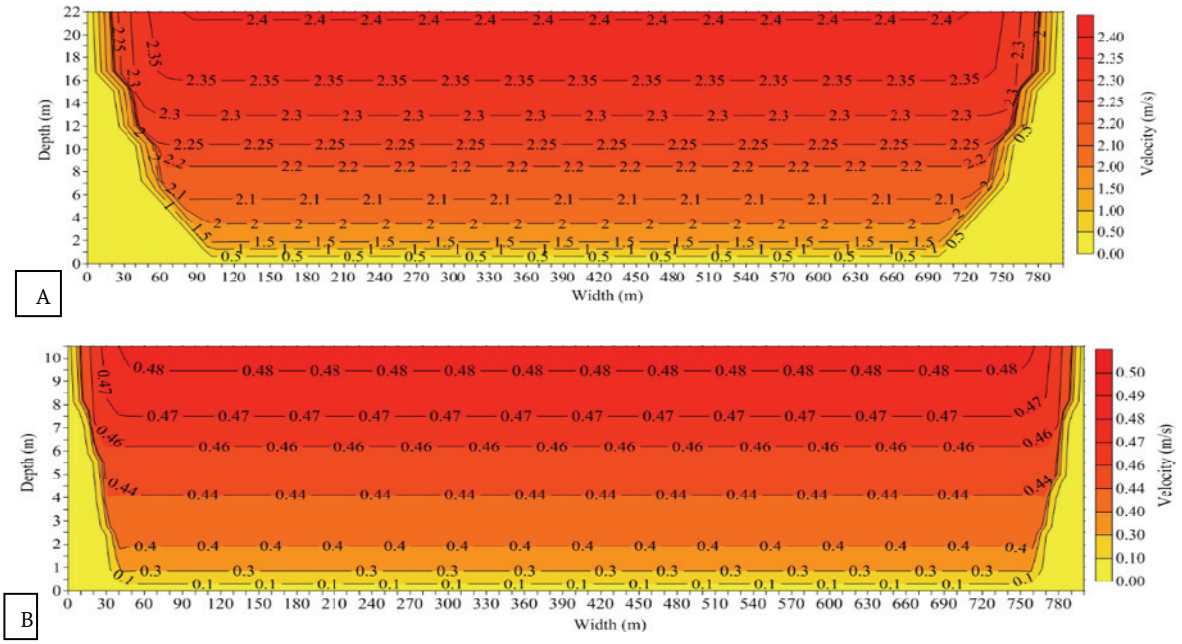

Figure 11. Isolines of velocity of the cross section of the Madeira River for the higher flow (A) and for the lower flow (B).

Figure 12A and B show the cross-sectional velocity profiles of the Tapajós River, which originate from the highest and lowest flow respectively. Thus, for the 22,530.0 $m^3 s^{-1}$ flow rate, the simulated mean velocity was 1.07 m s^{-1}, and for the same flow, the observed mean velocity is 1.12 m s^{-1}, and for the flow rate of 2,349.71 m s^{-1}, the mean simulated velocity was 0.27 m s^{-1} and the observed velocity was 0.26 m s^{-1}. In the Tapajós River, tide influence also occurs, which contributes to the low velocity, both for the flood period and for the dry season.

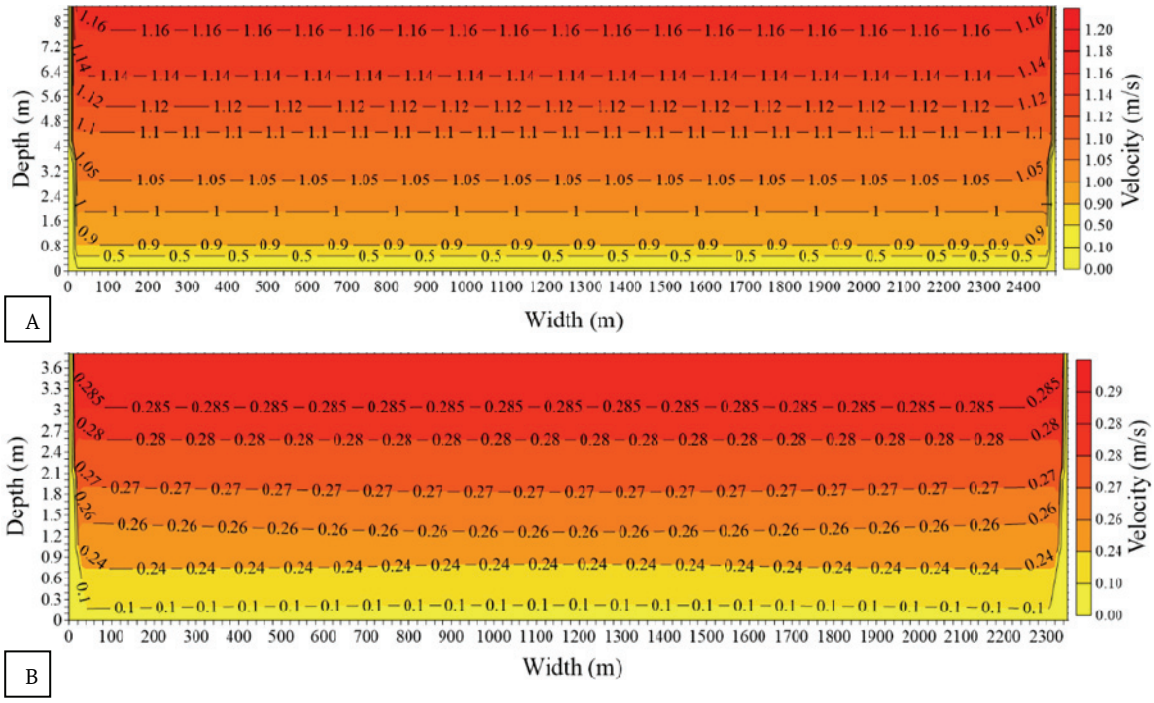

Figure 12. Isolines of the velocity of the cross section of the Tapajós River for the largest (A) and the lowest flow (B).

Figure 13A and B show the velocity profiles of the Xingu River cross section. The flow values (32,717.0 $m^3 s^{-1}$ and 617.0 $m^3 s^{-1}$) from the Altamira station (code: 18850000) gave rise to these velocity profiles. The simulated mean velocities were 1.41 m s^{-1} and 0.06 m s^{-1}, which were similar to the observed mean velocities of 1.38 m s^{-1} and 0.07 m s^{-1}, respectively.

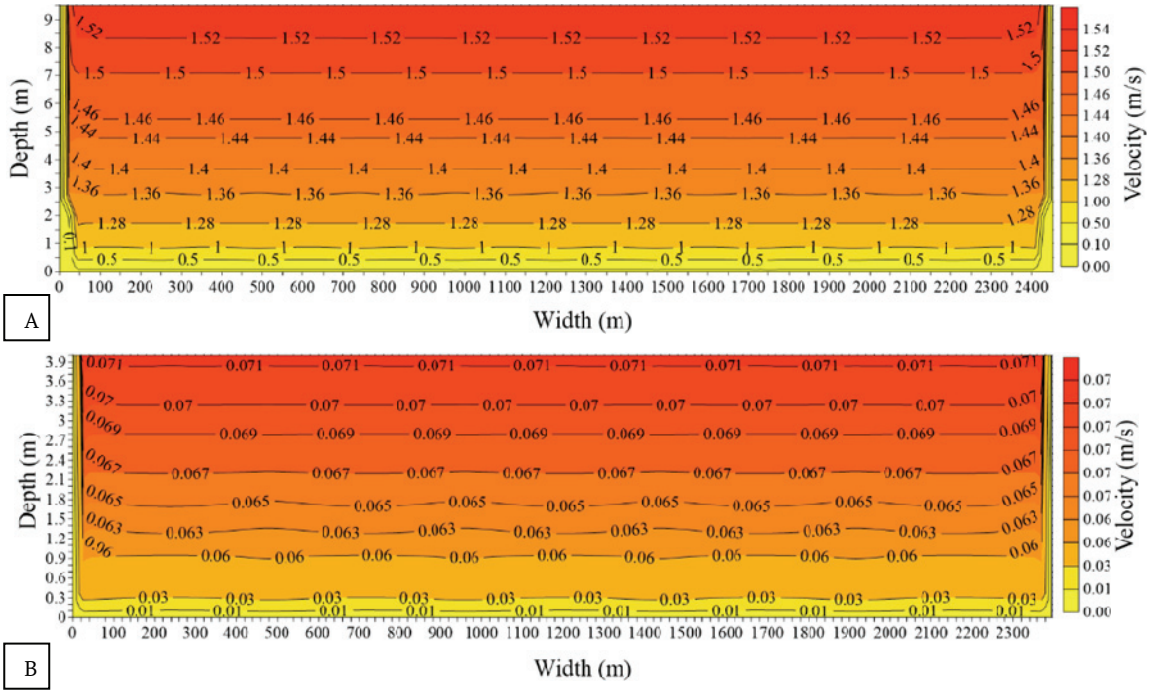

Figure 13. Isolines of the velocity of the cross section of the Xingu River for the largest (A) and for the lowest flow (B).

The results of the simulated mean velocities with flow values of the historical series (Table 2) for the main tributaries of the Amazon River show that the Trombetas, Madeira, and Xingu Rivers in their respective cross-sections of the Garganta, Palmeiral, and Altamira stations present higher average velocities than 2.0 m s^{-1} when the value used is the higher flow rate. The other rivers studied presented mean velocities within the range of 1.109 m s^{-1} to 1.788 m s^{-1}. However, when the values used are the lowest flow rates, the average velocities are between 0.024 m s^{-1} and 0.5 m s^{-1}, which are uninteresting for hydrokinetic energy generation.

Table 2. Results of the use of the flow-velocity model in the cross-sections of the streamflow gauge stations of the main tributaries of the Amazon River.

River	Station	Q_o (m^3 s^{-1})	Q_s (m^3 s^{-1})	Error (%)	U_o (m s^{-1})	U_s (m s^{-1})	Error (%)
Madeira	Palmeiral (Salto Jirau)	40,892.0	37,431.9	8.5	2.26	2.21	2.2
		3,705.0	3,528.6	4.8	0.46	0.44	4.3
Tapajós	Fortaleza	22,530.0	22,372.3	0.7	1.41	1.39	1.4
		2,349.7	2,332.4	0.7	0.27	0.26	2.2
Xingu	Passagem-Br	4,135.0	3,990.4	3.5	1.02	1.06	3.3
		568.0	560.3	1.3	0.32	0.32	1.6
	Boa Sorte	11,385.0	10,951.4	3.8	1.30	1.34	3.2
		488.0	481.8	1.3	0.14	0.13	6.6
	São Felix Do Xingu	13,982.0	13,816.0	1.2	1.25	1.24	0.4
		622.0	621.1	0.1	0.31	0.31	1.0
	Altamira	32,717.0	32,328.6	1.2	1.38	1.41	1.8
		617.0	611.0	1.0	0.07	0.06	5.9
Negro	Cucuí	10,347.0	9,724.4	6.0	1.22	1.18	3.1
		523.0	509.1	2.7	0.21	0.17	15.9
	Curicuriari	24,509.2	23,668.0	3.4	1.31	1.34	2.1
		1,251.0	1,242.6	0.7	0.22	0.23	7.4
	Serrinha	35,205.4	34,273.0	2.6	1.25	1.26	0.6
		4,306.0	4,247.6	1.4	0.32	0.32	1.2
Trombetas	Garganta	4,592.4	4,209.5	8.3	1.28	1.29	0.8
		47.0	45.3	3.7	0.04	0.04	0.0
Jari	São Francisco	3,866.6	3,705.7	4.2	1.19	1.18	0.4
		52.0	50.4	3.0	0.04	0.04	0.5

Q_o – observed flow; Q_s – simulated flow, U_o – observed mean velocity and U_s – simulated mean velocity.

Hydrokinetic potential estimation

Table 3 presents the hydrokinetic power inventory for all stations shown in Figure 2, using turbines with a diameter estimated from the lowest depth and power coefficients of 0.25 and 0.593. In the two turbine efficiency scenarios (Cp = 0.25 and Cp = 0.593), in all sections studied, the Amazon River has the highest hydrokinetic potential for both the higher flow and the lower flow. However, turbine installations on the Amazon River must respect the multiple uses of water, especially the navigability of the river, which is the main route of people traffic and freight transportation in the region.

Filizola et al. (2015) carried out a preliminary analysis of hydrokinetic potential in the Amazon basin, classifying the points studied in Itacoatiara and Óbidos as good-excellent, with the potential for the generation of energy close to one year, and in Manacapuru, it was classified as good for being able to generate energy 50% of the year. The Negro, Trombetas, Cachorro, Javari, Içá, Juruá, Coari, and Tapajós Rivers due to the greater velocities presented hydrokinetic potential that can be explored during the region's flood period, but in the dry season, the hydrokinetic powers are smaller than 0.1 kW. However, these are cases that cannot be ruled out, especially the Trombetas River, which for a higher flow can generate 105.8 kW of power with a turbine of 4.2 m in diameter. With this power being converted into electrical energy and made available to the riverside communities, it is possible to reduce the environmental impacts caused by the use of fossil fuel, contributing to the economic development of local communities. The Maracá River hydrokinetic turbine project is an example of the use of this technology in favour of the isolated communities in the Amazon. The power generated by the hydrokinetic turbine of 1 kW was used to meet the productive demand of an extractive nut community (Sánchez, Torres, & Kalid, 2015).

For the Tapajós and Jari Rivers, the installation of three hydroelectric plants is planned each river. On the Jari River, there already exists a hydroelectric plant. The streamflow gauge stations 17500000 and 19150000 (ANA codes), used to apply the model, will be downstream of the Chacorão and Açaipé B

hydroelectric plants, respectively. Once the dams are built, the flow dynamics of the river will be altered. Thus, future studies will be needed to determine the magnitudes of the velocities.

Table 3. Hydrokinetic powers of the cross-sections of the rivers of the Amazon basin used in the study.

Station code	River	depth (m)	U (m s^{-1})	Swept area (m^2)	Diameter (m)	Power (kW) (Cp = 0.25)	Power (kW) (Cp = 0.59)
17050001	Amazonas	50.0	2.329	397.4	22.5	627.6	1488.6
		40.0	0.753	397.4	22.5	21.2	50.3
10100000	Solimões/Amazonas	25.0	2.034	65.0	9.1	68.4	162.2
		16.0	0.794	65.0	9.1	4.1	9.6
16030000	Solimões/Amazonas	38.0	1.639	208.6	16.3	114.8	272.3
		28.5	0.801	208.6	16.3	13.4	31.8
14100000	Amazonas	30.0	1.621	56.7	8.5	30.2	71.6
		15.0	0.891	56.7	8.5	5.0	11.9
10500000	Javari	14.5	1.250	3.1	2.0	0.8	1.8
		3.5	0.270	3.1	2.0	0.0	0.0
11444900	Putomayo/Içá	13.0	1.305	4.2	2.3	1.2	2.7
		4.0	0.277	4.2	2.3	0.0	0.0
12200000	Juntaí	8.5	1.110	1.0	1.1	0.2	0.4
		2.0	0.366	1.0	1.1	0.0	0.0
12520000	Juruá	10.5	1.514	0.2	0.5	0.1	0.2
		1.0	0.480	0.2	0.5	0.0	0.0
13100000	Coari	6.5	0.777	1.3	1.3	0.1	0.2
		1.5	0.234	1.3	1.3	0.0	0.0
13962000	Purus	25.0	1.788	56.7	8.5	40.5	96.1
		15.0	0.277	56.7	8.5	0.2	0.4
14110000	Negro	12.5	1.350	3.1	2.0	1.0	2.3
		3.5	0.181	3.1	2.0	0.0	0.0
14330000	Negro	14.0	1.471	3.1	2.0	1.2	3.0
		3.5	0.222	3.1	2.0	0.0	0.0
14420000	Negro	14.0	1.248	6.6	2.9	1.6	3.8
		5.0	0.257	6.6	2.9	0.0	0.0
15400000	Madeira	23.0	2.340	132.6	4.0	20.1	47.7
		7.0	0.574	12.6	4.0	0.3	0.7
16430000	Trombetas	7.5	2.954	6.6	2.9	21.3	50.5
		5.0	0.024	6.6	2.9	0.0	0.0
16440000	Cachorro	9.3	1.394	6.6	2.9	2.2	5.3
		5.0	0.073	6.6	2.9	0.0	0.0
17500000	Tapajós	9.0	1.162	11.3	3.8	2.2	5.3
		4.0	0.308	11.3	3.8	0.0	0.1
18430000	Xingu	8.5	1.109	3.1	2.0	0.5	1.3
		3.7	0.326	3.1	2.0	0.0	0.0
18460000	Xingu	12.0	1.474	6.2	2.8	2.5	5.8
		5.0	0.134	6.2	2.8	0.0	0.0
18510000	Xingu	8.0	1.447	0.5	0.8	0.2	0.5
		1.4	0.308	0.5	0.8	0.0	0.0
18850000	Xingu	9.0	2.112	0.4	0.7	0.5	1.1
		1.2	0.249	0.4	0.7	0.0	0.0
19150000	Jari	8.0	1.424	2.3	1.7	0.8	1.9
		3.0	0.026	2.3	1.7	0.0	0.0

The Porto Velho streamflow gauge station (code: 15400000), located downstream of the Santo Antônio hydroelectric plant on the Madeira River, has an installed capacity of 47.7 kW, for the highest flow rate using a turbine with a diameter of 4 m and *Cp* equal to 0.593, and for the dry season, using the same turbine configuration, the power is 0.7 kW. For a turbine with *Cp* equal to 0.25, the power is 20.1 kW and 0.3 kW for the flood and dry season, respectively. As the power in the dry season is less than 1 kW, the hydrokinetic potential can be used during the flood period, and the diameter can be increased from 4 to 13 m; hence the power would increase from 47.7 to 504 kW, in the best scenario. By comparison, in a system consisting of a

Francis turbine with 50 kW of power and a mini grid of approximately 2 km, the small hydro power plant project in the Aruã fall provides electricity to 50 residences and for some productive uses (Sánchez et al., 2015). Therefore, the remaining potential of this hydroelectric plant could meet a demand ten times greater than the small hydropower plant mentioned.

The cross sections of the Xingu River have hydrokinetic potential for the higher flow, but for the lower flow, they did not present a good hydrokinetic potential. The Altamira stream gauge station (code: 18850000), the nearest (155 km upstream) to the Belo Monte hydroelectric plant, had installed power using a turbine with a diameter of 0.7 m and *Cp* of 0.593, giving 1.1 kW for the higher flow rate and 0.002 kW for the lower flow rate. In the case of use only during the flood period, the diameter can be increased to 5 m, so the power will increase to 54.8 kW for *Cp = 0.593*. This potential was evaluated upstream, but in future work, using the flow-velocity model, this potential can be evaluated downstream of the Belo Monte hydro power station reservoir.

Therefore, the estimated hydrokinetic potential can give communities isolated from the Amazon access to electricity. Implementation of decentralized energy systems is a good economic and environmental alternative, which can replace diesel power generators, which are widely used by isolated communities in the Amazon. Another alternative for the use of this technology is to integrate it into the national grid. If the implementation is done by individuals, there is the option to sell the energy produced to the energy concessionaires.

Conclusion

The proposed model simulates daily average velocities in the Amazon basin. These velocities are between 0.02 m s^{-1} and 2.95 m s^{-1}. The width/depth ratio is high, contributing to low velocities. The Amazon has hydrokinetic potential to generate energy annually and its tributaries only during the flood period. The limitations of the work are: 1) not considering the overflow of the river; 2) does not simulate on the longitudinal axis; 3) the *Cp* used only considers the maximum and minimum efficiency of the turbines. As a possible application of the model, we can derive a velocity equation using non-linear regression, with simulated velocities as explanatory variable and flow as dependent variable.

Acknowledgements

The authors would like to thank the Coordination for the Improvement of Higher Education Personnel-Brasil (CAPES) - Finance Code 001. The second author would like to thank CNPq for funding research productivity grant (Process 304936/2015-4). We would like to thank the office for research (PROPESP) and Foundation for Research Development (FADESP) of the Federal University of Pará through grant no. PAPQ 2018.

References

Agência Nacional de Água [ANA]. (2017). *Sistema de Informações Hidrológicas-HidroWeb*. Retrieved on Dec. 10, 2017 from http://www.snirh.gov.br/hidroweb/publico/apresentacao.jsf

Babaeyan-Koopaei, K., Ervine, D., Carling, P., & Cao, Z. (2002). Velocity and turbulence measurements for two overbank flow events in River Severn. *Journal of Hydraulic Engineering-Asce*, *128*(10), 891–900. DOI: 10.1061/(asce)0733-9429(2002)128:10(891)

Barros, M. L. C., & Rosman, P. C. C. (2018). A study on fish eggs and larvae drifting in the Jirau reservoir, Brazilian Amazon. *Journal of the Brazilian Society of Mechanical Sciences and Engineering*, *40*(2), 1-16. DOI: 10.1007/s40430-017-0951-1

Betz, A. (1926). *Windenergie und ihre Ausnutzung durch Windmühlen*. Germany: Ökobuch Verlag.

Bjerklie, D. M. (2007). Estimating the bankfull velocity and discharge for rivers using remotely sensed river morphology information. *Journal of Hydrology*, *341*(3-4), 144-155. DOI: 10.1016/j.jhydrol.2007.04.011

Bonakdari, H. (2012). Establishment of relationship between mean and maximum velocities in narrow sewers. *Journal of Environmental Management*, *113*, 474-480. DOI: 10.1016/j.jenvman.2012.10.016

Chen, Z., Wang, Z., Liu, Y., Wang, S., & Leng, C. (2016). Estimating the flow velocity and discharge of ADCP unmeasured area in tidal reach. *Flow Measurement and Instrumentation*, *52*(C), 208-218. DOI: 10.1016/j.flowmeasinst.2016.10.009

Farina, G., Bolognesi, M., Alvisi, S., Franchini, M., Pellegrinelli, A., & Russo, P. (2017). Estimating discharge in drainage channels through measurements of surface velocity alone: A case study. *Flow Measurement and Instrumentation*, *54*, 205-209. DOI: 10.1016/j.flowmeasinst.2017.02.006Get rights and content

Filizola, N., & Guyot, J. L. (2011). Fluxo de sedimentos em suspensão nos rios da Amazônia. *Revista Brasileira de Geociências*, *41*(4), 566-576. DOI: 10.25249/0375-7536.2011414566576

Filizola, N., Melo, E., Armijos, E., & McGlynn, J. (2015). *Preliminary analysis of potential for river hydrokinetic energy technologies in the Amazon basin*. Washington D.C.: Inter-American Development Bank.

Goring, D. G., Walsh, J. M., Rutschmann, P., & Trösch, J. (1997). Modelling the distribution of velocity in a river cross-section. *New Zealand Journal of Marine and Freshwater Research*, *31*(2), 155-162. DOI: 10.1080/00288330.1997.9516754

Holanda, P. S., Blanco, C. J. C., Mesquita, A. L. A., Brasil Junior, A. C. P., Figueiredo, N. M., Macêdo, E. N., & Secretan, Y. (2017). Assessment of hydrokinetic energy resources downstream of hydropower plants. *Renewable Energy*, *101*(C), 1203-1214. DOI: 10.1016/j.renene.2016.10.011

Holdefer, A. E., & Severo, D. L. (2015). Análise por ondaletas sobre níveis de rios submetidos à influência de maré. *Revista Brasileira de Recursos Hídricos*, *20*(1), 192-201. DOI: 10.21168/rbrh.v20n1.p192-201

Keulegan, G. H. (1938). Laws of turbulent flow in open channels. *Journal of Research of the National Bureau of Standards*, *21*(6), 707-741. DOI: 10.6028/jres.021.039

Kolekar, N., & Banerjee, A. (2015). Performance characterization and placement of a marine hydrokinetic turbine in a tidal channel under boundary proximity and blockage effects. *Applied Energy*, *148*(1), 121-133. DOI: 10.1016/j.apenergy.2015.03.052

Kosuth, P., Callède, J., Laraque, A., Filizola, N., Guyot, J. L., Seyler, P., ... Guimarães, V. (2009). Sea-tide effects on flows in the lower reaches of the Amazon River. *Hydrological Processes*, *23*, 3141-3150. DOI: 10.1002/hyp.7387

Kumar, D., & Sarkar, S. (2016). A review on the technology, performance, design optimization, reliability, techno-economics and environmental impacts of hydrokinetic energy conversion systems. *Renewable and Sustainable Energy Reviews*, *58*, 796-813. DOI: 10.1016/j.rser.2015.12.247

Laws, N. D., & Epps, B. P. (2016). Hydrokinetic energy conversion: Technology, research, and outlook. *Renewable and Sustainable Energy Reviews*, *57*, 1245-1259. DOI: 10.1016/j.rser.2015.12.189

Lee, H., Lee, C., Kim, Y., Kim, J., & Kim, W. (2013). Power law exponents for vertical velocity distributions in natural rivers. *Journal of Engineering*, *5*(12), 933-942. DOI: 10.4236/eng.2013.512114

Lopes, J. J. A., Vaz, J. R. P., Mesquita, A. L. A., Mesquita, A. L. A., & Blanco, C. J. C. (2015). An approach for the dynamic behavior of hydrokinetic turbines. *Energy Procedia*, *75*, 271-276. DOI: 10.1016/j.egypro.2015.07.334

Maghrebi, M. F. (2006). Application of the single point measurement in discharge estimation. *Advances in Water Resources*, *29*(10), 1504-1514. DOI: 10.1016/j.advwatres.2005.11.007

Maghrebi, M. F. & Ahmadi, A. (2017). Stage-discharge prediction in natural rivers using an innovative approach. *Journal of Hydrology*, *545*, 172-181. DOI: 10.1016/j.jhydrol.2016.12.026

Maghrebi, M. F., Ahmadi, A., Attari, M. & Maghrebi, R. F. (2016). New method for estimation of stage-discharge curves in natural rivers. *Flow Measurement and Instrumentation*, *52*(1), 67-76. DOI: 10.1016/j.flowmeasinst.2016.09.008

Maghrebi, M. F., & Rahimpour, M. (2005). A simple model for estimation of dimensionless isovel contours in open channels. *Flow Measurement and Instrumentation*, *16*(6), 347-352. DOI: 10.1016/j.flowmeasinst.2005.07.001

Meade, R. H., Rayol, J. M., Conceição, S. C., & Natividade, J. R. G. (1991). Backwater effects in the Amazon River of basin. *Environmental Geology and Water Sciences*, *18*(2), 105–114. DOI: 10.1007/BF01704664

Pektas, A. O. (2015). Computational modeling with sensitivity analysis: case study velocity distribution of natural rivers. *Neural Computing and Applications*, *26*(7), 1653-1667. DOI: 10.1007/s00521-015-1830-2

Petrie, J., Diplas, P., Gutierrez, M., & Nam, S. (2014). Characterizing the mean flow field in rivers for resource and environmental impact assessments of hydrokinetic energy generation sites. *Renewable Energy*, *69*, 393-401. DOI: 10.1016/j.renene.2014.03.064

Punys, P., Adamonyte, I., Kvaraciejus, A., Martinaitis, E., Vyciene, G., & Kasiulis, E. (2015). Riverine hydrokinetic resource assessment. A case study of a lowland river in Lithuania. *Renewable and Sustainable Energy Reviews*, *50*, 643-652. DOI: 10.1016/j.rser.2015.04.155

Rahimpour, M. (2017). Dimensionless isovelocity contours in rectangular cross sections by harmonic mean distances. *ISH Journal of Hydraulic Engineering*, *23*(3), 241-245. DOI: 10.1080/09715010.2016.1277796

Rahimpour, M., & Maghrebi, M. F. (2006). Prediction of stage-discharge curves in open-channels using a fixed-point velocity measurement. *Flow Measurement and Instrumentation*, *17*(5), 276-281. DOI: 10.1016/j.flowmeasinst.2006.07.001

Sánchez, A. S., Torres, E. A., & Kalid, R. A. (2015). Renewable energy generation for the rural electrification of isolated communities in the Amazon Region. *Renewable and Sustainable Energy Reviews*, *49*, 278-290. DOI: 10.1016/j.rser.2015.04.075

Sivapragasam, C., & Muttil, N. (2005). Discharge rating curve extension - A new approach. *Water Resources Management*, *19*(5), 505-520. DOI: 10.1007/s11269-005-6811-2

Van Els, R. H., & Brasil Junior, A. C. P. (2015). The brazilian experience with hydrokinetic turbines. *Energy Procedia*, *75*, 259-264. DOI: 10.1016/j.egypro.2015.07.328

Vermaak, H. J., Kusakana, K., & Koko, S. P. (2014). Status of micro-hydrokinetic river technology in rural applications: A review of literature. *Renewable and Sustainable Energy Reviews*, *29*, 625-633. DOI: 10.1016/j.rser.2013.08.066

Yuce, M. I., & Muratoglu, A. (2015). Hydrokinetic energy conversion systems: A technology status review. *Renewable and Sustainable Energy Reviews*, *43*(3*)*, 72-82. DOI: 10.1016/j.rser.2014.10.037.